

## A novel absorptive/reflective solar concentrator for heat and electricity generation: An optical and thermal analysis



Xian-long Meng<sup>a,f</sup>, Nazmi Sellami<sup>g,\*</sup>, Andrew R. Knox<sup>b</sup>, Andrea Montecucco<sup>b</sup>, Jonathan Siviter<sup>b</sup>, Paul Mullen<sup>b</sup>, Ali Ashraf<sup>b</sup>, Antonio Samarelli<sup>b</sup>, Lourdes F. Llin<sup>b</sup>, Douglas J. Paul<sup>b</sup>, Wen-guang Li<sup>b</sup>, Manosh C. Paul<sup>b</sup>, Duncan H. Gregory<sup>c</sup>, Guang Han<sup>c</sup>, Min Gao<sup>d</sup>, Tracy Sweet<sup>d</sup>, Robert Freer<sup>e</sup>, Feridoon Azough<sup>e</sup>, Robert Lowndes<sup>e</sup>, Xin-lin Xia<sup>f</sup>, Tapas K. Mallick<sup>a,\*</sup>

<sup>a</sup> Environment and Sustainability Institute, University of Exeter, Penryn Campus, TR10 9FE, UK

<sup>b</sup> School of Engineering, University of Glasgow, Glasgow G12 8QQ, UK

<sup>c</sup> School of Chemistry, University of Glasgow, Glasgow G12 8QQ, UK

<sup>d</sup> School of Engineering, Cardiff University, Cardiff CF24 3AA, UK

<sup>e</sup> School of Materials, University of Manchester, Manchester M13 9PL, UK

<sup>f</sup> School of Energy Science & Engineering, Harbin Institute of Technology, Harbin 15001, China

<sup>g</sup> School of Engineering and Physical Sciences, Heriot-Watt University, Dubai Campus, Dubai International Academic City, PO Box: 294345, Dubai, United Arab Emirates

### ARTICLE INFO

#### Article history:

Received 26 November 2015

Accepted 4 February 2016

#### Keywords:

Solar concentrator

Absorption

Reflection

Optical efficiency

### ABSTRACT

The crossed compound parabolic concentrator (CCPC) is one of the most efficient non-imaging solar concentrators used as a stationary solar concentrator or as a second stage solar concentrator. In this study, the CCPC is modified to demonstrate for the first time a new generation of solar concentrators working simultaneously as an electricity generator and thermal collector. The CCPC is designed to have two complementary surfaces, one reflective and one absorptive, and is named as an absorptive/reflective CCPC (AR-CCPC). Usually, the height of the CCPC is truncated with a minor sacrifice of the geometric concentration. These truncated surfaces rather than being eliminated are instead replaced with absorbent surfaces to collect heat from solar radiation. The optical efficiency including absorptive/reflective part of the AR-CCPC was simulated and compared for different geometric concentration ratios varying from  $3.6\times$  to  $4\times$ . It was found that the combined optical efficiency of the AR-CCPC  $3.6\times/4\times$  remained constant and high all day long and that it had the highest total optical efficiency compared to other concentrators. In addition, the temperature distributions of AR-CCPC surfaces and the assembled solar cell were simulated based on those heat flux boundary conditions. It was shown that the addition of a thermal absorbent surface can increase the wall temperature. The maximum value reached 321.5 K at the front wall under  $50^\circ$  incidence. The experimental verification was also adopted to show the benefits of using absorbent surfaces. The initial results are very promising and significant for the enhancement of solar concentrator systems with lower concentrations.

© 2016 The Authors. Published by Elsevier Ltd. This is an open access article under the CC BY-NC-ND license (<http://creativecommons.org/licenses/by-nc-nd/4.0/>).

### 1. Introduction

Renewable energy offers a valuable solution to the challenges facing energy security and also plays an important role in the reduction of global warming. It is well known that solar energy is the most promising in all renewable and clean energy resources. The commercialization of high efficiency solar cells faces major challenges owing to the high costs. The concentrated photovoltaic

(CPV) modules are capable of collecting sunlight onto solar cells by the use of optical concentrators thereby reducing the required cell area per unit of output power [1]. The cost of CPV modules could be reduced by increasing the output per unit solar cell and this could be achieved by replacing the expensive solar cells with a low cost optical material [2], such as using Fresnel lens [3], refractive mirrors based on the total internal reflections [4], the reflective imaging [5] and non-imaging (CPC type) solar concentrators [6]. Among the recent technological innovations, building integrated photovoltaic system (BIPV) has become a hotspot technology [7]. In BIPV, the window, skylights and roof of buildings are replaced by transparent CPV materials [6,8]. In this way some building costs can be

\* Corresponding authors.

E-mail addresses: [Solarnaz@gmail.com](mailto:Solarnaz@gmail.com) (N. Sellami), [t.k.mallick@exeter.ac.uk](mailto:t.k.mallick@exeter.ac.uk) (T.K. Mallick).

### Nomenclature

CCPC	crossed compound parabolic concentrator	BIPV	building integrated photovoltaic
AR-CCPC	absorptive/reflective CCPC	UDF	user-defined functions
$C_g$	geometric concentration ratio	$\rho$	density ( $\text{kg}/\text{m}^3$ )
$\lambda$	heat conductivity ( $\text{W}/(\text{m}^2 \text{K})$ )	$T_s$	wall temperature (K)
$C_p$	specific heat capacity ( $\text{J}/(\text{kg K})$ )	$S$	energy source term
CPV	concentrated photovoltaic		

saved; meanwhile the building itself is maintained as a free support. For these reasons, the BIPV has been recognized as a great potential way to bring a faster development stage for solar energy [9].

Non-imaging optics aims to provide the widest possible acceptance angles and therefore, is the most appropriate for solar concentration [10,11]. The idea was expanded by Winston and Gordon [12], and has become widely used in BIPV area in recent years [7]. Compound parabolic concentrators (CPC) consists of two parabolic mirror segments with different focal points and it is the most traditional 'ideal' non-imaging collector [13]. Neither a '2-D' nor a '3-D' CPC, however, can satisfy the requirement of modularity perfectly with square entry and exit solar cells. Therefore, the CCPC structure appears to be a satisfactory solution which is formed by the perpendicular intersection of two 2-D CPC troughs [8,14].

A full size CPC has the highest concentration, the upper-most part is, however, nearly parallel to the optical axis and therefore contributes very little. The truncation method has been adopted to balance the relationship between concentration and mirror area. For a traditional CPC, the optimal position for truncation is about half of the full height [15]. The  $4\times$  CCPC structure with a half acceptance angle of  $30^\circ$ , truncated to provide a concentration of  $3.6\times$ , was found to have a more effective performance as a static solar concentrator [6,8].

A problem remains, however, with an increase in the temperature of the solar cells assembled to the concentrators [16]. In a CPV system, only part of the received solar energy can be transferred into electricity (typical efficiencies for monocrystalline cells are 16–24% [17,18], and for polycrystalline cells 14–18% [19]), and the remainder causes a temperature rise within the cell junctions. The current study aims to provide a solution to increase the total

efficiency of the CPV system by maximising the thermal collection which can be stored for local heat transfer. It has been proved that hybrid CPV/thermal (CPV/T) systems have the advantage of satisfying different demands including thermal and electrical energy [20–22]. The CPV/T modules can capture the remaining thermal energy and remove the waste heat from the PV module thus improve the total energy utilisation ratio [23–25].

In this article, a novel CPV system which still retains the full height of the CCPC is proposed. The CCPC is modified to produce for the first time a new generation of solar concentrators simultaneously working as a CPV and as a solar heat source. This concept is designed to have two complementary surfaces, one reflective and one absorbent, called Absorbent/Reflective CCPC (AR-CCPC). The optical efficiencies including absorptive/reflective part of this AR-CCPC are simulated and compared for different geometric concentration ratios varying from  $3.6\times$  to  $4\times$ , achieved by varying the degree of truncation. Experimental verification is also performed to show the benefits of using absorbent surfaces. These initial results are very promising and significant for the enhancement of solar concentrator systems with lower concentrations.

## 2. Model description

The AR-CCPC module proposed for modelling and testing is presented in Fig. 1. It was manufactured using thermally conductive material, composed of a thermal absorption part and an optical reflection part. As previously mentioned, the height of the CCPC is typically truncated with a minor sacrifice of the geometric concentration. In this study, these truncated surfaces are, rather eliminated, replaced with absorbent surfaces in order to collect heat from the solar radiation. The upper portion is covered by

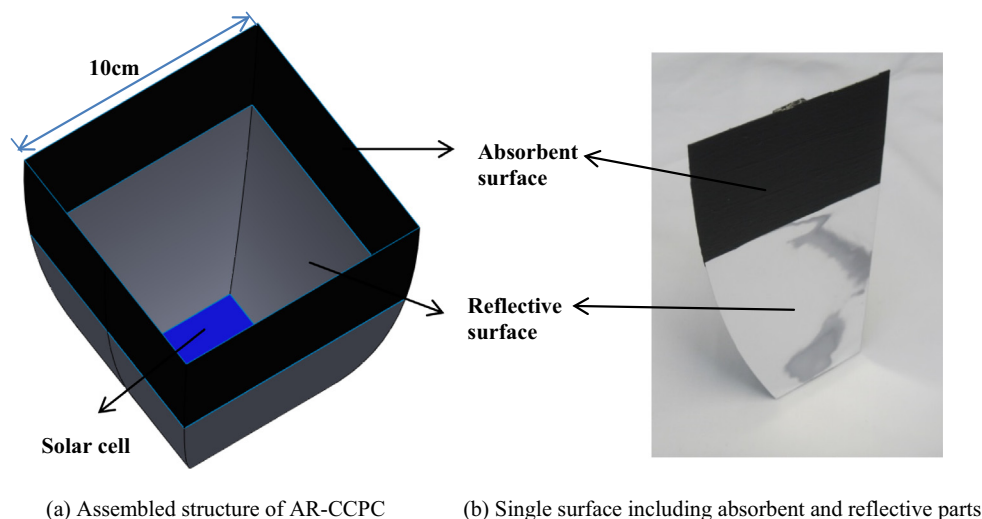


Fig. 1. The geometrical structure of the AR-CCPC for modelling and testing.

non-reflective paint which has an absorptive rate of  $\alpha$  equal to 0.94. The lower portion has the reflectivity  $\rho = 0.94$  and serves to collect sunlight onto the 50 mm  $\times$  50 mm square exit aperture of the AR-CCPC where the solar cell is placed. The benefits are:

- The surfaces near the top (full height), which would ordinarily be truncated, are being replaced by absorption material to be used for heat transfer. The addition of thermal absorbent walls can improve the total optical efficiency at all incidences. The absorbent walls may block some of solar rays especially at low incidence so that reduce the PV output. The total optical efficiency keeps high at all incidences.
- Some of the reflected and scattered rays from the bottom and the environment can be recycled by the upper-most part of the absorber. This effect will be apparently enhanced when the incidence angle of the incoming rays increases.

The key parameter for AR-CCPC is the geometrical concentration ratio  $C_g$ , which can be defined as the ratio of the top entry area to the bottom area:

$$C_g = A_{in}/A_{out} \tag{1}$$

where  $A_{in}$  and  $A_{out}$  represent the entrance area for incident solar rays and the exit area for the solar cell, respectively. It is directly determined by the selected acceptance angle and the degree of truncation [8,26], i.e., assigned height of each part.

The totally reflective CCPC of full height (when the surfaces are totally parallel to the optical axis) with 30° incident angle has a  $C_g$  of 4.0. Understandably, the solar energy reaching the bottom panel

decreases with an increasing proportion of upper-part truncation. In this paper, a ray tracing technique via APEX software is adopted to evaluate the optical characteristics for each part. APEX optics is an add-in software for SOLIDWORKS and it can present the energy transmission process during optical design system. Point sun model was mainly used in the simulations to show it more clearly. Other than that, the realistic sun source is considered in discussing the flux distribution on solar cell. Different AR-CCPC under  $C_g$  of reflective surfaces of between 3.6 $\times$  to 3.9 $\times$  will be investigated with the purpose of enhancing the total optical efficiency to thermal/PV. Cases under 3.5 $\times$  would not have a big impact, therefore they are ignored.

The optical efficiency can be defined as:

$$Eff_{optical} = N_{received}/N_{in} \tag{2}$$

Note that  $N_{received}$  represents the number of received solar rays on the target surfaces, which can be both the thermal absorbent walls and the solar cell.  $N_{in}$  is the number of input parallel rays on the entrance area. It is no doubt that with the increase of sampled solar rays, the solving accuracy can be improved, but at the same time the simulation becomes more time-consuming. In the current simulations,  $N_{in}$  is set to be 10<sup>6</sup>.

Fig. 2 demonstrates the path of the incident rays simulated using ray tracing technique in the APEX software. The paths of the solar rays are highly variable at different incident angles. To show it more clearly, some schematic drawings for a single ray are also shown at the side. For convenience, the front

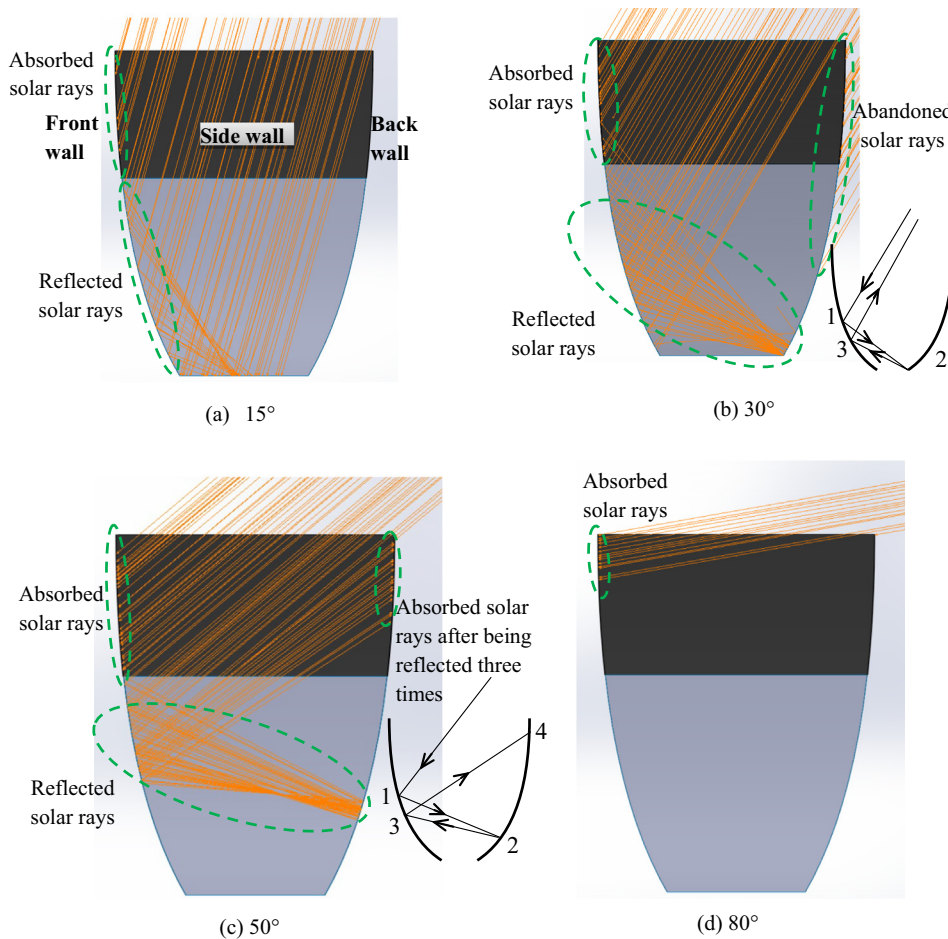


Fig. 2. The ray tracing of the AR-CCPC concept simulated by APEX software at different incident angles.

surface is defined as the one that directly face towards the incident direction. The opposite is then named as the back wall and the others the side walls. In order to represent an assembled array, the solar rays hitting the exterior walls of single module would not contribute for the energy conversion. Both the thermally absorbent surfaces and the solar cell at the bottom can receive sun rays when the incident angles are lower than 30°. Beyond this angle, the thermal absorbent component contributes alone; the solar cell is “cut-off” from the incident radiation. The sun rays are reflected three times by the mirrors. Some of them escape out of the concentrator, but another part hit the back wall and increase the temperature, such as Fig. 2(c) shows at 50° incidence. In addition, the energy captured by the front wall, even if the angle increases to 80°, is still non-zero.

The AR-CCPC is designed to have two complementary surfaces: one reflective and one absorbent. In order to maximize the total energy output, these two surfaces were divided via truncation at an appropriate height to provide a reflector with a concentration ranging from 3.6 to 3.9. The absorbent part is complementary to make the total concentration of the AR-CCPC 4×. Fig. 3 presents the dimensions including the length of the bottom of the solar cells, and the cutting method at different dividing heights, so that the different concentrations from 3.6× to 4.0× can be obtained. Once the size of entry square is determined by formula (1), the height can be obtained through drawing programs. 3.6×/4× in the figure represents truncating a full height of a 4× CCPC by a down-part reflector with 3.6× concentration.

### 3. Results and discussions

#### 3.1. Performance of reflective part

The optical performance of the reflective part is investigated in the current section. Fig. 4 presents the optical efficiencies of different AR-CCPC and totally reflective CCPC. For the sake of comparison, the 3.6× CCPC is the truncated down part of 3.6×/4× AR-CCPC. The resulting modules are close-packed to avoid bypassing available sunlight. Due to its larger acceptance angle, the totally reflective 3.6× CCPC provides a higher efficiency and wider incident tolerance when compared with  $C_g$  of 4×. The absorbent walls being used or not, the optical efficiency of full height 4× CCPC decrease dramatically at the accept angle of 30°.

On the other hand, the addition of absorbent walls collects the heat instead of reflecting it. The obtained thermal energy will increase if the reflective part becomes smaller, so the PV optical efficiency will reduce. The 3.9×/4× AR-CCPC assembled structure, for instance, has the maximum optical efficiency of 91%. However, the corresponding optical efficiency value of 3.6×/4× AR-CCPC is lower (about 85%). Owing to the blockings of the thermal absorption surfaces, the concentrated sunlight would be reduced more as the angle of incidence grows from 0° to 30°. The decreased efficiency could reach 25% before a sharper decrease at the edge. The

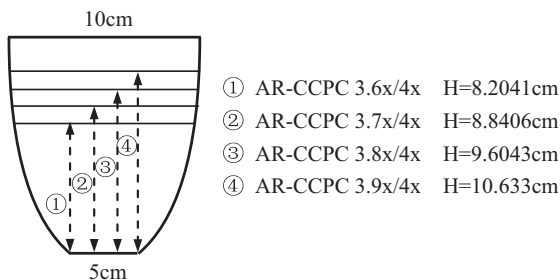


Fig. 3. Different types of AR-CCPC by changing the dividing height.

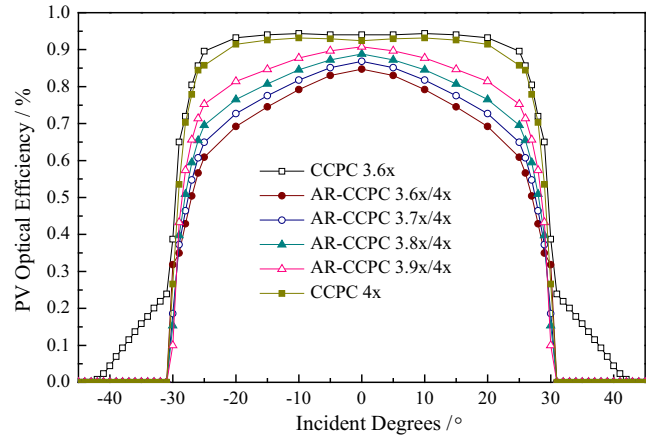


Fig. 4. A comparison of the optical efficiencies of the different AR-CCPCs and totally reflective CCPCs.

PV optical efficiency of the 3.6×/4× AR-CCPC drops from 84.7% (at 0°) to 60.7% (at 25°).

Fig. 5 shows the obtained concentration distribution of the solar cell. A point sun model does not make big difference for the optical efficiencies. However, it would make the peak flux on solar cell much higher, which is against the practical situation. Here the realistic sun source with 4.65 mrad half angle is considered, which is more practical. About 40% of normal incident solar rays directly hit the central positions of the solar cell, except four hotspots which exist around the edge. This causes the maximum flux to reach a peak of 17×. These hotspots can be located at different positions depending on the incident angle. At an incident angle of 15°, the hotspots exist around the middle, and the peak flux reaches nearly 28 suns. High temperatures generate resistive losses within the cell and then decreases the PV conversion efficiency [27,28]. Adding the cooling devices for CPV modules, therefore, has become a common solution [29,30]. Another solution, instead of rejecting heat, is that the residual thermal energy can be collected for local heat transfer. The solar cells can firstly be cooled down by an inlet of cold water. And the second-stage heat transfer happens at the absorbent walls so that increases the water temperature further. The AR-CCPC system will provide two main advantages to increase the total efficiency of the CPV module:

- Cooling of the solar cells, therefore increasing their electrical efficiency and lifetime.
- Collection of thermal energy for local heating.

#### 3.2. Performance of thermal absorbent surfaces and combinative model

In the following analysis, the incident direct beam radiation will be taken as 1000 W/m<sup>2</sup>. Table 1 demonstrates the absorptive and reflective rates for each optical material: the high reflecting film used for the reflective part and the non-reflective paint used for the thermal receiving walls. The wavelength factor had been omitted, allowing the properties to be simplified to grey-body. The suited wavelength of the reflecting film is higher than 400 nm which covers most of the incoming energy. For the absorbent paint, the wavelength of high absorptivity ranges from 400 nm to 1400 nm.

The optical efficiencies of thermal absorbent surfaces are shown in Fig. 6. For all the types, the efficiencies of the thermal walls are less than 10% when exposed at 0° direct sunlight since the effective irradiance areas are rather small. However, we can find that the efficiencies rise rapidly under higher incident degrees. The optical

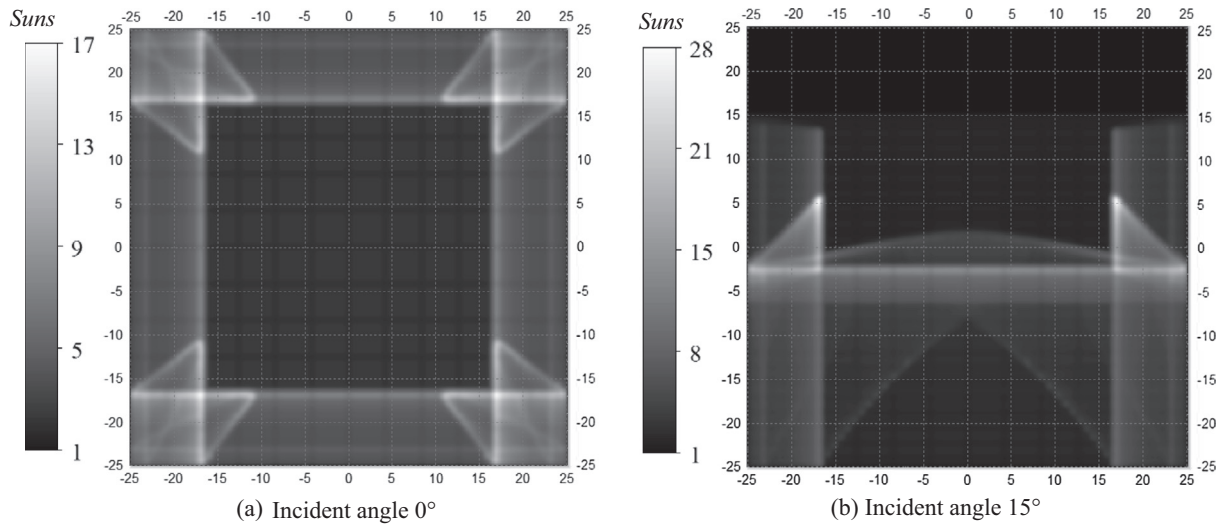


Fig. 5. The 2-D flux distributions of 3.6×/4× AR-CCPC at different incident angles, when the realistic sun model with a 4.65 mrad half angle is adopted.

Table 1  
Optical properties of the materials used in the simulations.

Used optical materials	Reflective rate	Absorptive rate	Suited wavelength
High-reflecting film	0.94	0.06	>400 nm
Non-reflective paint	0.06	0.94	400–1400 nm

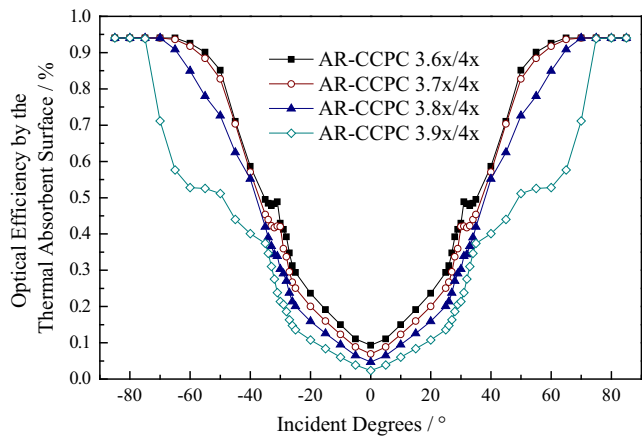


Fig. 6. A comparison of the optical efficiency by the thermal absorbent surface at different concentrations.

efficiency of 3.6×/4× and 3.7×/4× AR-CCPC could reach nearly 94% at around 65–85°, because the transmission path of solar rays is similar to the case in Fig. 2(d). Nearly all the incident solar rays are redirected onto the back walls. Fig. 6 also clearly demonstrates the comparison of thermal contributions at different  $C_g$ . 3.6×/4× AR-CCPC obviously achieves the most heat flux for thermal use. The 3.9×/4× AR-CCPC type, however, performs least well with an efficiency much lower than the others. In addition, the fluctuation phenomenon between 30° and 60° is caused by the multi-reflections by the reflective walls.

For a better understanding of the thermal characteristics for the absorbent part, the 2-D distributions of simulated absorbed rays by the absorbent walls under 50° incidence are demonstrated in Fig. 7. The origin of the coordinate system here locates at the centre of the

solar cell (xoy plane), which is perpendicular to the z-axis. The front wall (see Fig. 7(a)) which is facing towards the sun receives a fully smooth flux around 900 W/m<sup>2</sup>. At the bottom edge there is a steadily increasing tendency due to the impact of reflected rays. Because of the multiple reflections, the middle of back wall (see Fig. 7(b)) collects more rays which makes the peak flux reach 1000 W/m<sup>2</sup>. As the flux comes from the narrower and lower reflecting surface (see Fig. 2(c)), the flux area of back thermal wall is not fully covered. Interestingly, the incident angle can influence the position and length of the flux distribution along z-axis. A larger incidence angle moves the focal spot downwards. Compared with the other walls, the side wall produces little heat at high incident angles. The gradient shape is due to the incident inclined angle. Similar to the front wall, the energy flux increases from top to bottom.

The statistics of total received power including thermal absorbent and reflective contributions are presented in Fig. 8. For the case of 4× CCPC, the peak energy at 0° is 9.3 W, which is higher than the same position of the 3.6× CCPC at 8.5 W. The disadvantage of the CCPC 4× lies in its narrow tolerance for incidence which is only 30°. It therefore misses some solar rays under high incidences. In contrast, the received energy by AR-CCPC makes a large improvement. Both the thermal absorbent and reflective parts contribute to the total power.

The total flux of each type remains nearly the same within the maximum range of acceptance angle. Beyond this angle, the proportion of thermal energy dominates. Fig. 8 demonstrates the large fluctuations occurring between 30° and 85°. The total received energy decreases dramatically between 30° and 35°, which has the lowest electric output and relatively low thermal energy. The total energy then peaks at 50° and continues to decrease. During this range the back absorption surface could also obtain some reflected solar rays from the front wall. When the angle is 50°, the thermal energy received from the back wall reaches its maximum value, resulting the peak total output. The thermal power then decreases dramatically from 50° to 85°. The total energy of the AR-CCPC at  $C_g = 3.6×/4×$ , on the whole, maintains a better optical performance at all incident angles and offers the best performance.

The total optical efficiency is a key parameter to be evaluated, which can be defined by this formula:

$$\text{Total optical efficiency} = Eff_{pv} + Eff_{thermal} \quad (3)$$

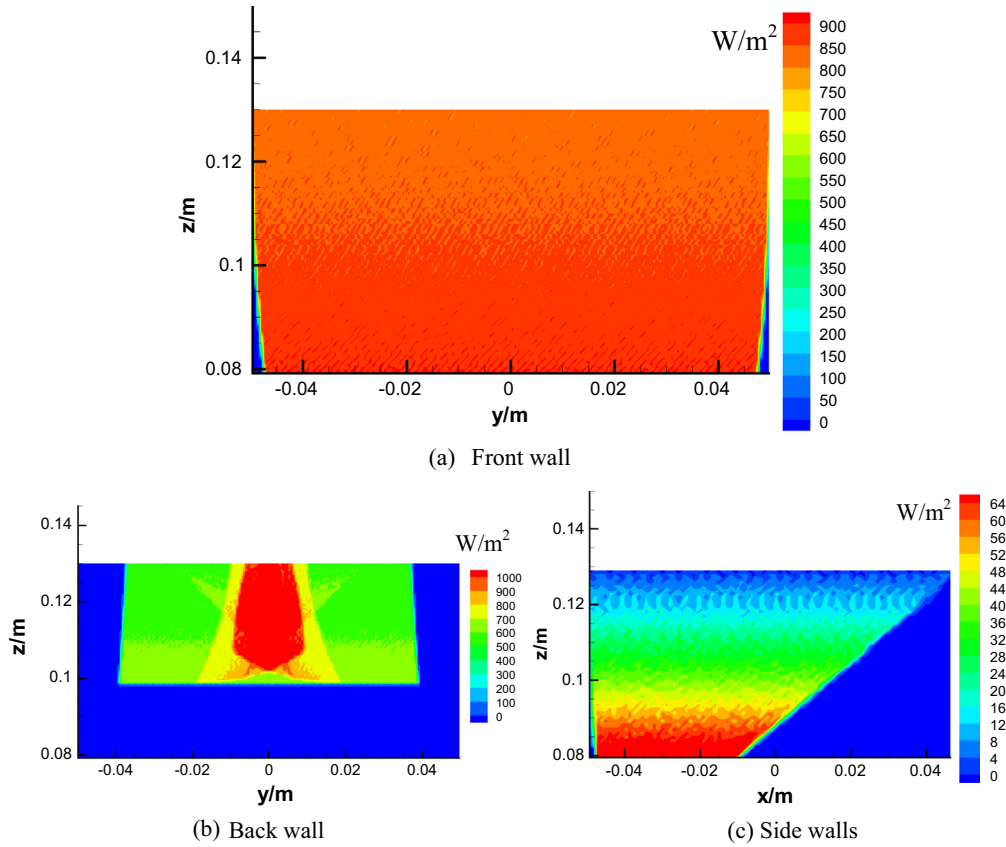


Fig. 7. The 2-D absorbed solar rays on the thermal absorber walls with an incident angle of 50°, for 3.6×/4× AR-CCPC. When the external irradiance is 1000 W/m<sup>2</sup>.

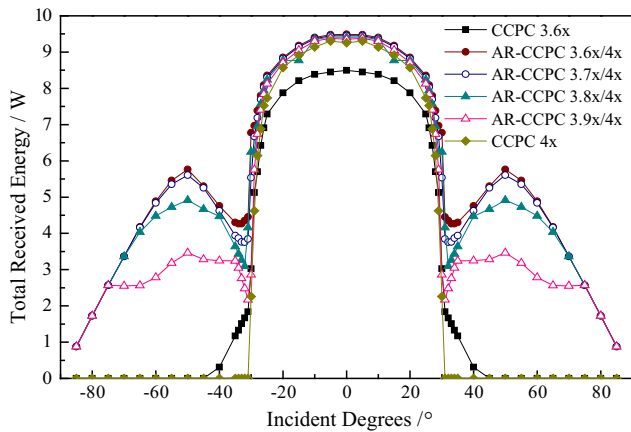


Fig. 8. A comparison of the total received energy of the AR-CCPC with the totally reflective CCPC.

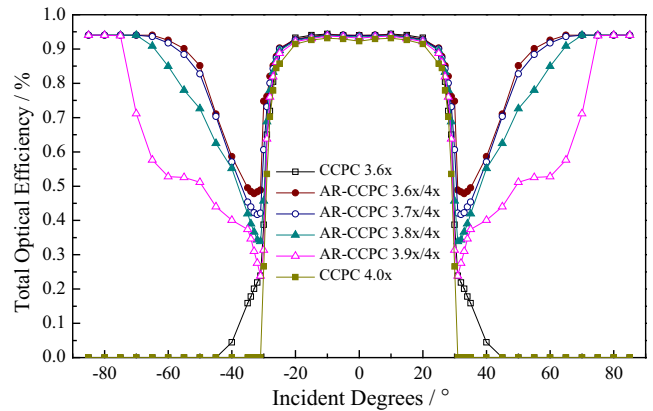


Fig. 9. The total optical efficiency of the AR-CCPC at different concentrations.

where  $Eff_{pv}$  and  $Eff_{thermal}$  represent the optical efficiency generated from the reflective and thermal absorber surfaces, respectively. Also, the simulation results are based on the optical properties provided in Table 1.

Fig. 9 presents the simulated total optical efficiencies at different  $C_g$  and incident angles. Within the acceptance angle, the limited reflectivity of the reflective surfaces maintains the optical efficiency at around 94%. Above the acceptance angle of 30°, the concentrated solar rays for the solar cells fall off sharply. Hence both the reflective and thermally absorber parts contribute little between 30° and 35° and the total efficiency is at the minimum compared with other incident angles. When beyond 35°, there is

a noticeable upward trend as fewer rays escape with the increase of the incident angle. The total efficiency reaches nearly 94% above 60° for 3.6×/4× AR-CCPC, which indicates that nearly all of the incident rays are absorbed.

Solar rays strike buildings from different directions continually at different times of the day. To investigate the effect of arbitrary solar incidence, the optical efficiency along the diagonal of CCPC has been compared, as Fig. 10 shows. The module selected for study was 3.6×/4× AR-CCPC. The performance of the CCPC 3.6× with 30° acceptance angle [8] is also added to be compared. It was found that it matched well with the AR-CCPC results especially within 30° incident angle. Beyond this angle, however, the AR-CCPC module is able to receive more heat flux than CCPC. It

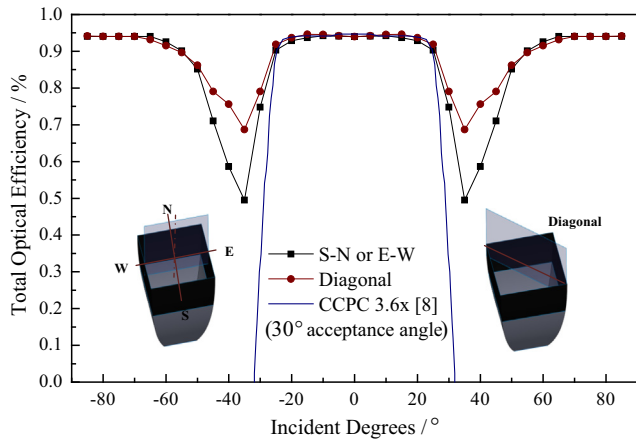


Fig. 10. A comparison of the total optical efficiency of 3.6×/4× AR-CCPC under different incident directions.

shows that the efficiency variation between S–N and the diagonal planes is large between 25° and 55° incidence. At 35°, for instance, the total efficiency in the diagonal plane reaches 68.7% which is much higher than the S–N direction (49.5%). The key reason is that the diagonal direction has a higher tolerance of the incidence for the optical efficiency [8]. It is interesting to note that 55° is a critical point. Beyond this angle, the S–N plane produces slightly higher total efficiency. For the other incident ranges, the total efficiencies of diagonal direction rays are the same compared with the S–N or E–W directions. As expected, the total efficiency is around 94% within the range from 0° to 20°, and 70° to 85°.

3.3. Performance of the thermal heat transfer for AR-CCPC

For the AR-CCPC module, the temperature distributions of absorbent surfaces and the solar cell represent the thermal absorption capability as well as the working performance. Here the 3-D

Table 2 Physical properties of different materials used.

Materials	Density (kg/m <sup>3</sup> )	Specific heat capacity (J/kg K)	Thermal conductivity (W/m K)	Radiation emissivity
Aluminium sheet	2719	871	202.4	0.09
Silicon rubber	1030	1100	0.14	Ignored
Single crystal silicon	2330	712	130	0.667 [32]

temperature distributions on the thermally absorbent surfaces and solar cell were simulated by ANSYS FLUENT software [31]. Supposing that the physical properties of materials used were homogeneous and unchanged with temperature, the steady governing equation for all the surfaces of AR-CCPC module would be solved:

$$\nabla(\rho c_p T_s) = \nabla \cdot (\lambda \nabla T_s) + S \tag{4}$$

$\rho$ ,  $c_p$ ,  $\lambda$  refers to the density, specific heat and thermal conductivity of different materials.  $T_s$  refers to the temperature. These physical properties are shown in Table 2.

$S$  represents the energy source term and can be treated as the sum of natural convection  $S_{conv}$ , boundary heat flux  $S_{rad}$  and heat dissipation source term  $S_w$ :

$$S = S_{conv} + S_{rad} + S_w \tag{5}$$

The physical properties of different materials used in the present work are presented in Table 2. The radiation emissivity of a silicon solar cell and commercial aluminium sheet are treated as 0.667 [32] and 0.09 [33], respectively. According to the actual experimental condition, the room temperature is set as 308 K. The heat transfer coefficient for the natural convection of air is 10 W/(m<sup>2</sup> K).

Fig. 11 presents the assembled AR-CCPC module. The system includes three basic components: AR-CCPC module, solar cell and the silicon rubber. All the surfaces of AR-CCPC are continually exposed at the parallel solar rays (and some multi-reflected rays). The four walls are thermally connected at their edges. The silicon rubber plays important role of electrical encapsulation. The top of the solar cell requires to be coated with this encapsulation material. The diffused light has been ignored in the current study because the experiment was taken under room conditions. In order to guarantee the accuracy of simulation results, the obtained ray tracing data as described above are treated as the heat flux boundary condition with the aid of UDF, which is the user defined function of FLUENT software and can freely change or add any source items in the energy equation.

The heat flux of thermal absorbent walls are totally different under various incident degrees. The natural convection loss and radiation loss have been considered. The boundary conditions used for temperature simulation are presented in Table 3. It is worth mentioning that a large contact thermal resistance exists between the AR-CCPC and the silicon rubber. The interfaces here are only 1.5 mm which is the thickness of aluminium sheets.

For the silicon rubber, it can be considered as an ideally transparent material therefore both the incident heat flux and radiation loss were ignored. The natural convection loss, however, should be considered. The thermal contact resistance between the solar cell and silicon rubber must also be added as indicated in Fig. 11.

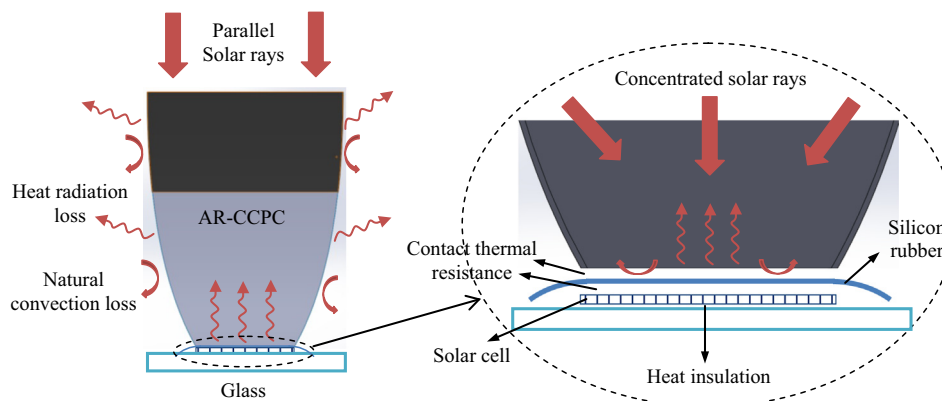


Fig. 11. The sketch of assembled AR-CCPC.

**Table 3**

The boundary conditions for the heat transfer simulation.

Components	Concentrated heat flux	Radiation loss	Natural convection loss	Contact thermal resistance
AR-CCPC	Yes	Yes	Yes	With silicon rubber
Silicon rubber	No	No	Yes	With AR-CCPC & solar cell
Solar cell	Yes	Yes	No	With silicon rubber

For the solar cell, the heat flux boundary is programmed according to the actual heat flux distribution as demonstrated in Fig. 5. The efficiency of the solar cell used here is treated as a constant which is 0.15. The residual power is the heat flux boundary which accounts for 0.85 of the total concentrated power. At the top of the solar cell, there is radiation loss and at the bottom a glass sheet which is considered as a thermal insulator.

The AR-CCPC surfaces are divided into finite mesh elements with the aid of the advanced size function of curvature in ANSYS FLUENT software. The mesh independency has been verified as Fig. 12 shows. Three mesh numbers including 1262, 5108 and 10096 with the same size function have been adopted. And the

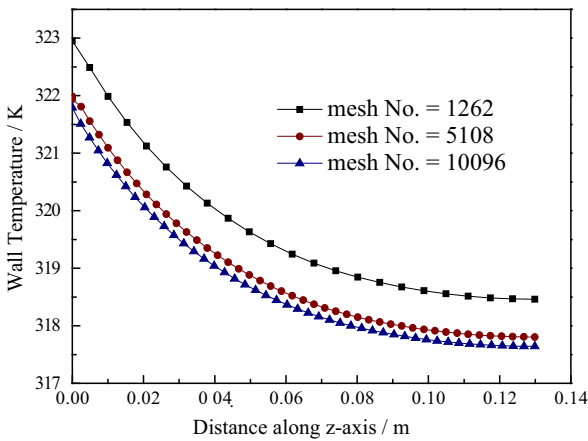
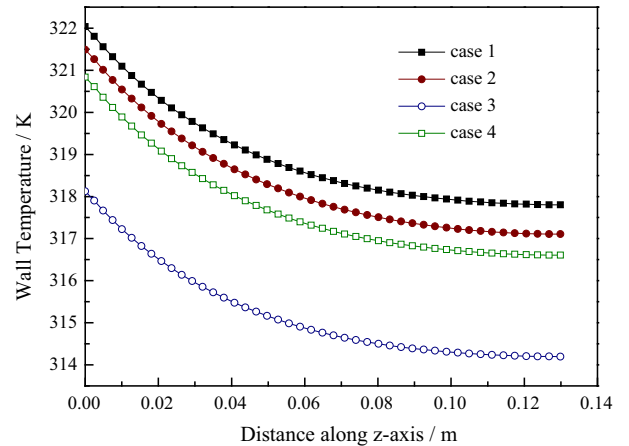


**Fig. 12.** Mesh independent verification for the simulations.

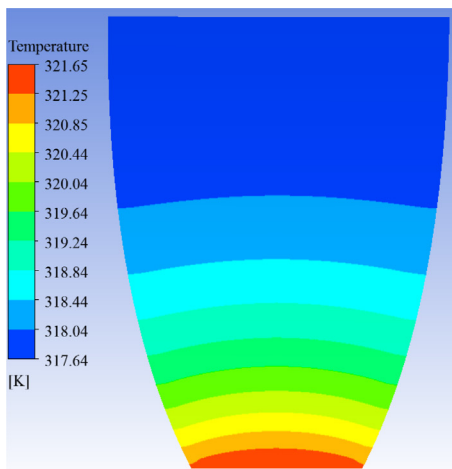
temperatures along the symmetry axis of AR-CCPC 3.6/4× front walls are compared. It can be found that the difference between 5108 and 10096 is only around 0.3 K. Therefore, 10096 mesh cells are enough in the current simulations. In addition, the convergence criterion is to be  $5 \times 10^{-7}$  relative error between consecutive iterations for the grid points in the calculation domain.

Fig. 13 shows the temperature distribution under 0° incidence under steady-state working condition. Since the AR-CCPC device is only 4 K. According to Fig. 13(a), the lowest temperature area lies on the top absorbent surface and it increases slowly from top to bottom, until reaching the solar cell edge that leads to a sharp temperature rise. These thin aluminium sheets provide a high thermal contact resistance with the solar cell which contributes to a large temperature gap. It is apparent from Fig. 13(b) that the highest temperature of solar cell is 371 K. And the centre position of the solar cell obtains a lower temperature of 367.6 K for the reason that the concentration ratio around the centre is only 1 sun and most of the heat in this area comes from the corners.

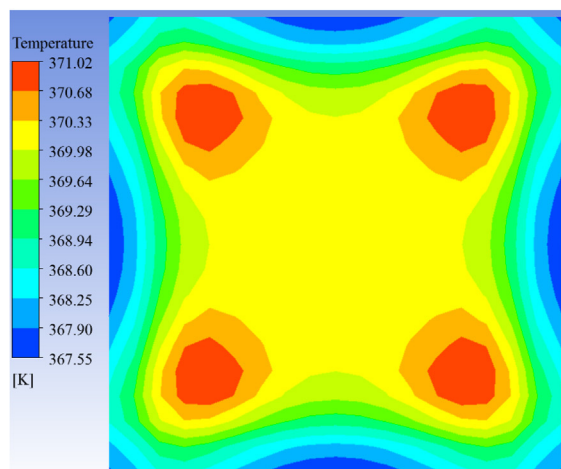
In order to investigate the influences of various parameters for the simulations, the front wall temperature of four cases were



**Fig. 14.** Sensitivity analysis of different solar irradiance, heat convection coefficient and radiation emissivity.



(a) AR-CCPC wall



(b) Assembled solar cell

**Fig. 13.** The isotherms across different components of AR-CCPC system under 0° incidence. Room temperature was 308 K. (a) is one of the AR-CCPC walls; (b) is the assembled solar cell at the bottom of the AR-CCPC. Here the heat flux boundary is based on the realistic sun model with a 4.65 mrad half angle.

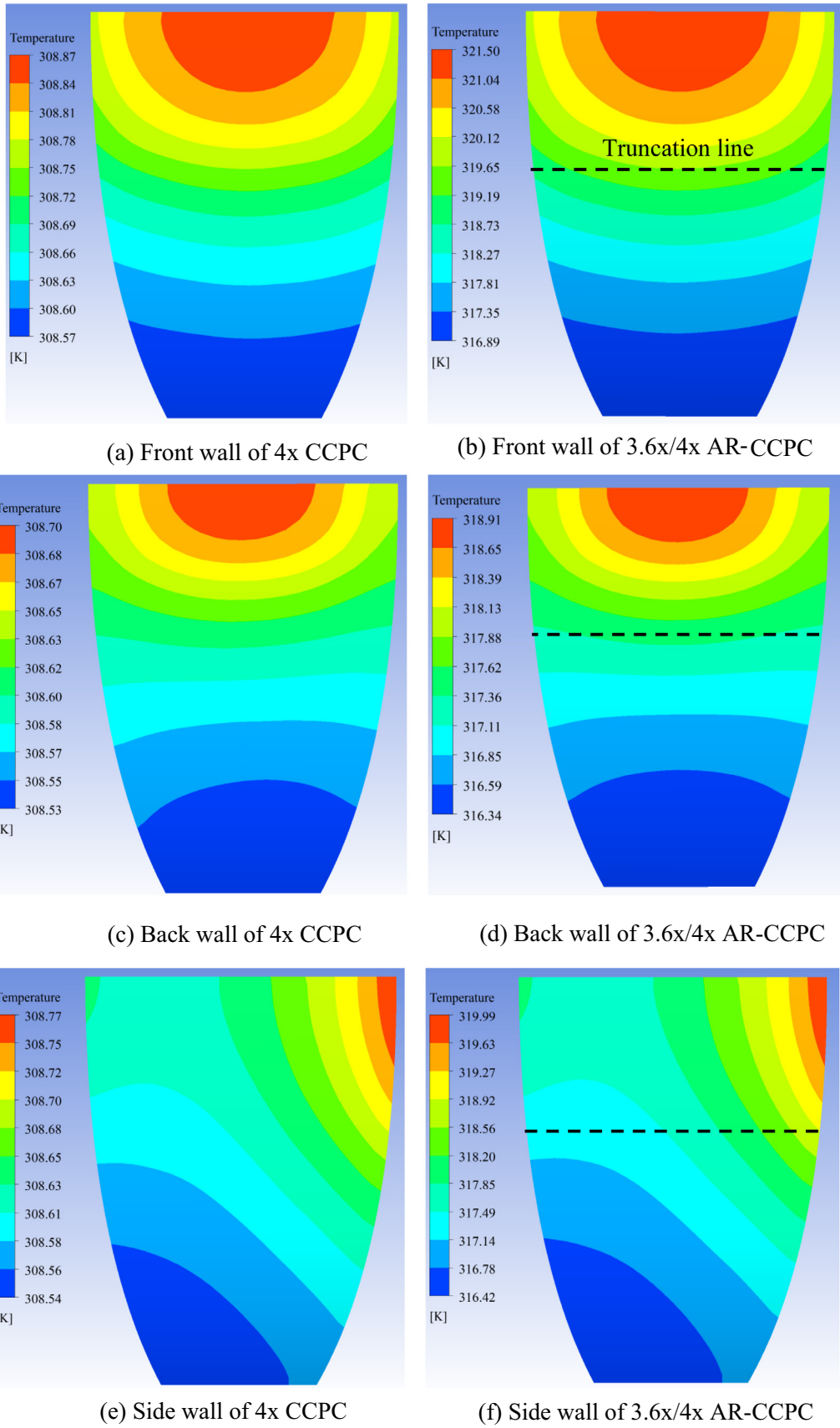


Fig. 15. A comparison of the wall temperatures of the 3.6x/4x AR-CCPC and the 4x CCPC under 50° incidence. Note that each figure has a different temperature scale.

compared in Fig. 14. Case 1 is based on the parameters of Table 2. Case 2 studies 600 W/m<sup>2</sup> solar irradiance. Case 3 changes the heat convection coefficient into 15 W/(m<sup>2</sup> K). Case 4 changes the radiation emissivity into 0.3. It is no doubt that all of the above cases can decrease the wall temperature. Compared with the others, the natural heat convections make the most difference which is nearly 4 K.

In order to illustrate the performance of thermally absorbent surfaces, the wall temperatures of the 3.6×/4× AR-CCPC and the 4× CCPC under 50° incidence are compared, as Fig. 15 demonstrates. The addition of thermally absorbent surfaces results in an increase in the wall temperatures. In Fig. 15(a), (c) and (e) the temperature of the total reflective CCPC is changed very slightly and the peak value reaches only 308.87 K which occurs on the top of front wall. For the AR-CCPC module, the maximum value also appears at the front wall, shown in Fig. 15(b) which is 321.5 K. Due to the highest heat flux on the upper-most absorbent surface, the temperature of the front wall peaks at the top and decreases by 5 degrees until the bottom. The solar cell cannot receive any solar rays based on the condition of 50° incident degrees, therefore the bottom temperatures are the lowest.

The highest temperature of the back wall, on the other hand, reaches 318.9 K. Owing to the smaller concentration area as shown in Fig. 7(b), the higher temperature mainly concentrates on the central area around the top of back wall. On the other hand, the temperature difference between the front and back wall apparently produces a cross-gradient distribution on the side wall, from the highest of 320 K to the lowest at 316.4 K. In general, all the surfaces of the AR-CCPC obtain a much higher temperature than the totally reflective CCPC. This demonstrates that the novel AR-CCPC module is able to improve the total efficiency.

The wall temperature of the AR-CCPC at different incident degrees has been measured as shown in Fig. 16. A solar simulator with quality AAA+ provides the 1000 W/m<sup>2</sup> solar density. Photovoltaic standards mandate that Class AAA+ solar simulators meet the demanding requirements in three key performance areas: spectral match to the solar spectrum, spatial non-uniformity of irradiance, and temporal instability of irradiance. The tested CPV system consists of an assembled AR-CCPC module and a plastic base with adjustable angle. The back side of the module has been covered with high reflective film for light blocking. The real-time temperature of the thermal absorbent walls have been monitored

by several thermocouples. There are four of thermocouples located at the left of every thermal wall, with 10 cm height and 3 cm distance from the edge. The electric power output was obtained by the I-V tracer. According to the measurements, the data reached the steady state within 20 min.

The measured electric power for  $C_g = 3.6\times$ ,  $C_g = 3.6\times/4.0\times$  and bare solar cell are shown and compared in Table 4. It can be seen that the electricity output was considerably improved with the aid of concentration. Because of the irregularity of the reflecting surface, the output electric power under 30° remains non-zero. The highest output reaches 1253 mW, obtained by the  $C_g = 3.6\times$  type under 0° incident angle. The results of  $C_g = 3.6\times/4.0\times$  type, on the other hand, show a certain decrease, especially at high incident angles. Nevertheless, it still received high improvement between 3.23 (at 0°) and 1.41 times (at 30°) compared with the bare solar cell.

The absorptive wall temperatures obtained by the simulations and measurements are compared based on different incident angles, as Fig. 17 shows. The measurement uncertainties have also been added. According to the simulation results, the wall temperature remains high before the acceptance angle of 30° due partly to the energy contribution from the solar panel. It decreases obviously around 30° when the largest number of solar rays have escaped. After that, the back wall receives the reflected solar rays from the front wall thus causing a peak thermal output of 50°. The average measurement results agree well with the simulations. However, the surface irregularity and reflection errors have caused the response delay of minimum/maximum value to some extent. The first minimum of the side wall temperature, for instance, appears at 40° when the simulation appears at 30°. The second crest of front and side wall temperature happens at 60°, which the simulation shows at 50°.

**Table 4**  
Output electric power (mW).

Incident angle (°)	Bare cell	$C = 3.6\times$	$C = 3.6\times/4.0\times$	Improvements (3.6×/4.0× vs bare cell)
0	380	1253	1229	3.23 times
10	383	1127	1087	2.84 times
20	363	954	777	2.14 times
30	343	573	483	1.41 times

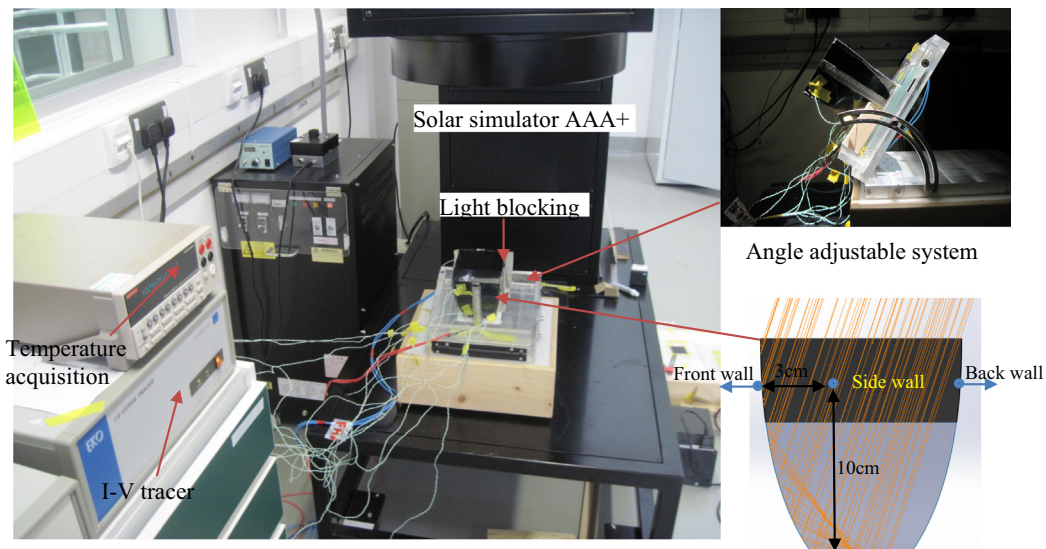


**Fig. 16.** Experimental setup for the AR-CCPC wall temperature analysis.

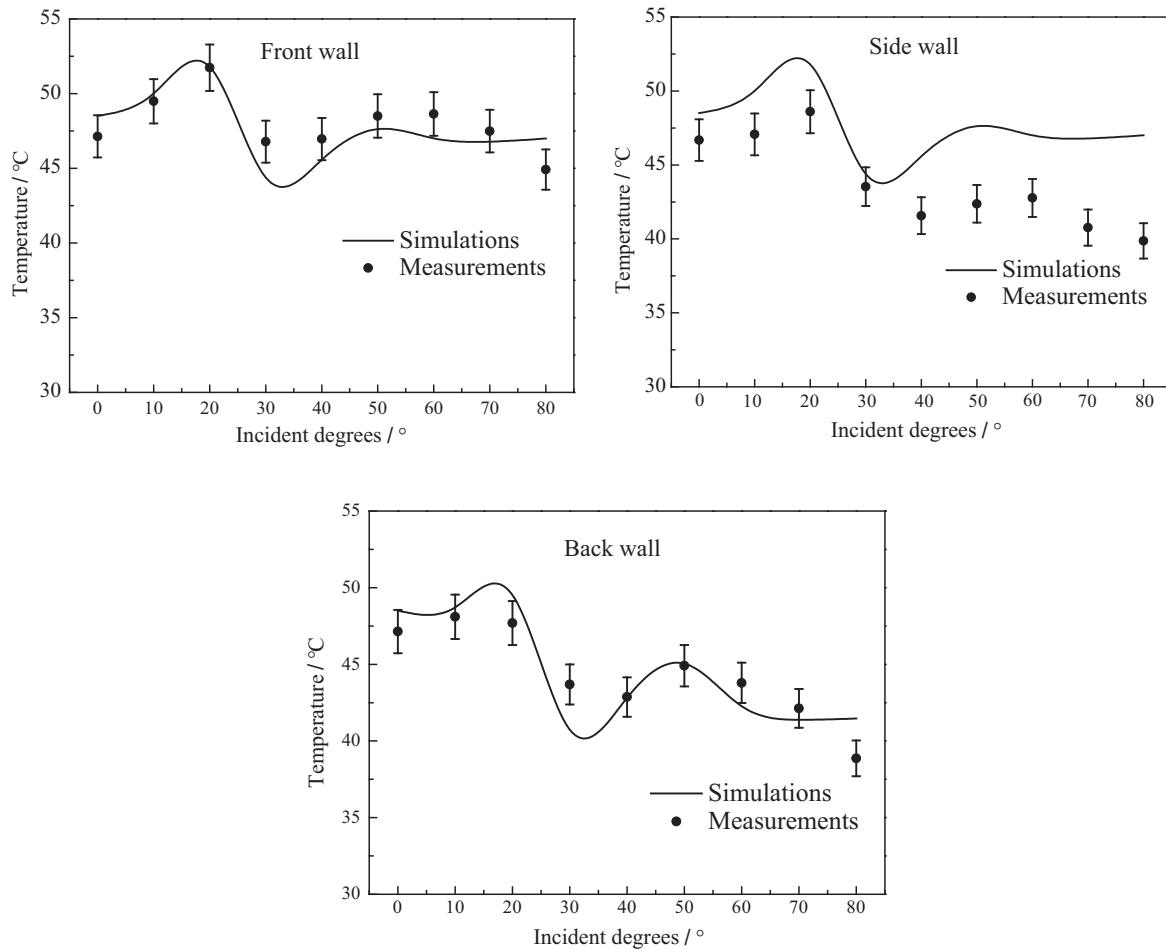


Fig. 17. Variation of measured absorbent wall temperatures.

#### 4. AR-CCPC embedded in PV/T hybrid system

The measurements have proved that the addition of an absorbent surface results in an increase to the wall temperature. These results indicate that this part of thermal energy can be utilized through water pipeline [34] surrounding the upper absorbent walls. The addition of upper absorbent walls is necessary in a practical concentrating PV/T hybrid system, as Fig. 18 shows. As designed, the thermal energy can be economically transported for local heat transfer.

Within the acceptance angle at noon time, the solar cell is under working condition and it can be firstly cooled down by the inlet of cold water. During this stage, the electricity output will be the dominant. The second-stage heating happens at the absorbent walls where the water temperature will increase further. The temperature rise may not be significant but the warm water can be stored in a tank for later use.

Exceeding the acceptance angle in the afternoon, only the absorbent walls keep heating the water. According to the simulations, the absorbent walls of each AR-CCPC (10 cm by 10 cm) receives 0.8 W (85° incidence) to 5.4 W (50° incidence). Although the input flux and delta T are both low, the heat transfer can be enhanced by using an array of modules covering larger area. For the same flow rate, more modules can be easier to reach a thermal equilibrium. The Building Integrated Concentrating Photovoltaic system, for instance, consists of several hundreds of CPV modules which could be a suitable platform.

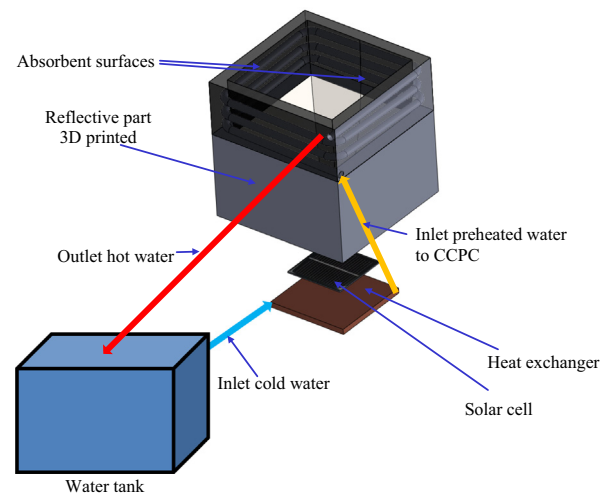


Fig. 18. AR-CCPC embedded in PV/T hybrid system.

A water tank combined with phase change techniques in the future study can enhance the thermal performance further. AR-CCPC modules provide a longer heat transfer duration. With the aid of phase change storage, the duration of hot water output can be dramatically extended.

## 5. Conclusion

The current study proposes a novel CPV concept that has been modified from the classic CCPC system, called AR-CCPC. The optical, thermal and total efficiency of the AR-CCPC module were simulated by APEX ray tracing software, and compared at different geometric concentration ratios varying from  $3.6\times$  to  $4\times$ . For the optical efficiency of the solar cell alone, the totally reflective  $3.6\times$  CCPC provides a higher efficiency and wider incident tolerance as compared with all the others. For the total efficiency including the thermal contributions, the  $3.6\times/4\times$  AR-CCPC was evaluated as having a higher optical efficiency at all incident angles.

In order to explore the potential for thermal heat transfer, a simple model of bare surface with no water flow was built. It showed that the addition of a thermal absorbent surface can apparently increase the wall temperature. The experimental verification was also performed and the results conform well with the simulations.

On the whole, these results are promising and significant for the enhancement of lower solar concentrator systems. The proposed system is suitable for building integrated system for combine thermal and electricity generation. As the next step, the water tubes designed according to the current performance data, need to be assembled surrounding the upper absorbent surfaces for the convective heat transfer. Based on a practical concentrating PV/T hybrid system, the thermal energy can be economically transported by AR-CCPC for local heat transfer.

## Acknowledgements

This work was financially support through EPSRC funded SUPERGEN Solar Challenge project SUNTRAP (EP/K022156/1) and China Scholarship Council (CSC) for Xianlong Meng's PhD funding.

## References

- [1] Meng XL, Xia XL, Sun C, Dai GL. Optimal design of symmetrical two-stage flat reflected concentrator. *Sol Energy* 2013;93:334–44.
- [2] Luque A, Sala G, Luque-Heredia I. Photovoltaic concentration at the onset of its commercial deployment. *Prog Photovolt* 2006;14:413–28.
- [3] Sonneveld P, Swinkels G, Van Tuijl B, Janssen H, Campen J, Bot G. Performance of a concentrated photovoltaic energy system with static linear Fresnel lenses. *Sol Energy* 2011;85:432–42.
- [4] Baig H, Sellami N, Chemisana D, Rosell J, Mallick TK. Performance analysis of a dielectric based 3D building integrated concentrating photovoltaic system. *Sol Energy* 2014;103:525–40.
- [5] Meng XL, Xia XL, Sun C, Hou XB. Adjustment, error analysis and modular strategy for Space Solar Power Station. *Energy Convers Manage* 2014;85:292–301.
- [6] Sellami N, Mallick TK, McNeil DA. Optical characterisation of 3-D static solar concentrator. *Energy Convers Manage* 2012;64:579–86.
- [7] Norton B, Eames PC, Mallick TK, Huang MJ, McCormack SJ, Mondol JD, et al. Enhancing the performance of building integrated photovoltaics. *Sol Energy* 2011;85:1629–64.
- [8] Sellami N, Mallick TK. Optical efficiency study of PV crossed compound parabolic concentrator. *Appl Energy* 2013;102:868–76.
- [9] Wei H, Liu J, Yang B. Cost-benefit comparison between domestic solar water heater (DSHW) and building integrated photovoltaic (BIPV) systems for households in urban China. *Appl Energy* 2014;126:47–55.
- [10] Chemisana D, Ignasi Rosell J. Design and optical performance of a nonimaging Fresnel transmissive concentrator for building integration applications. *Energy Convers Manage* 2011;52:3241–8.
- [11] Sarmah N, Richards BS, Mallick TK. Design, development and indoor performance analysis of a low concentrating dielectric photovoltaic module. *Sol Energy* 2014;103:390–401.
- [12] Winston R, Gordon J. Nonimaging optics: efficient design for illumination and solar concentration introduction. In: *Nonimaging optics: efficient design for illumination and solar concentration X*, vol. 8834; 2013. p. 1.
- [13] Hinterbe H, Winston R. Efficient light coupler for threshold Cerenkov counters. *Rev Sci Instrum* 1966;37. 1094–8.
- [14] Mammo ED, Sellami N, Mallick TK. Performance analysis of a reflective 3D crossed compound parabolic concentrating photovoltaic system for building facade integration. *Prog Photovolt* 2013;21:1095–103.
- [15] Rabl A. Comparison of solar concentrators. *Sol Energy* 1976;18:93–111.
- [16] Anderson WG, Dussinger PM, Sarraf DB, Tamanna S. Heat pipe cooling of concentrating photovoltaic cells. In: *PVSC: 2008 33rd IEEE photovoltaic specialists conference*, vols. 1–4. IEEE; 2008. p. 905–10.
- [17] Ebong A, Cooper IB, Rounsaville B, Tate K, Rohatgi A, Bunkenburg B, et al. High efficiency inline diffused emitter (ILDE) solar cells on mono-crystalline CZ silicon. *Prog Photovoltaics Res Appl* 2010;18:590–5.
- [18] Petter Jelle B, Breivik C, Drolsum Røkenes H. Building integrated photovoltaic products: a state-of-the-art review and future research opportunities. *Sol Energy Mater Sol Cells* 2012;100:69–96.
- [19] Wawer P, Müller J, Fischer M, Engelhart P, Mohr A, Petter K. Latest trends in development and manufacturing of industrial, crystalline silicon solar-cells. *Energy Proc* 2011;8:2–8.
- [20] Zhai H, Dai YJ, Wu JY, Wang RZ. Energy and exergy analyses on a novel hybrid solar heating, cooling and power generation system for remote areas. *Appl Energy* 2009;86:1395–404.
- [21] Kosmadakis G, Manolakos D, Papadakis G. Simulation and economic analysis of a CPV/thermal system coupled with an organic Rankine cycle for increased power generation. *Sol Energy* 2011;85:308–24.
- [22] Renno C, Petito F. Design and modeling of a concentrating photovoltaic thermal (CPV/T) system for a domestic application. *Energy Build* 2013;62:392–402.
- [23] Vivar M, Everett V, Fuentes M, Blakers A, Tanner A, Le Lievre P, et al. Initial field performance of a hybrid CPV-T microconcentrator system. *Prog Photovolt* 2013;21:1659–71.
- [24] Liu Y, Hu P, Zhang Q, Chen Z. Thermodynamic and optical analysis for a CPV/T hybrid system with beam splitter and fully tracked linear Fresnel reflector concentrator utilizing sloped panels. *Sol Energy* 2014;103:191–9.
- [25] Looser R, Vivar M, Everett V. Spectral characterisation and long-term performance analysis of various commercial heat transfer fluids (HTF) as direct-absorption filters for CPV-T beam-splitting applications. *Appl Energy* 2014;113:1496–511.
- [26] Mammo ED, Sellami N, Mallick TK. Performance analysis of a reflective 3D crossed compound parabolic concentrating photovoltaic system for building facade integration. *Prog Photovoltaics Res Appl* 2013;21:1095–103.
- [27] Najafi H, Woodbury KA. Optimization of a cooling system based on Peltier effect for photovoltaic cells. *Sol Energy* 2013;91:152–60.
- [28] Collin LM, Arenas OJ, Ares R, Frechette LG. Thermal resistance and heat spreading characterization platform for concentrated photovoltaic cell receivers. *IEEE Trans Compon Packag Manuf Technol* 2013;3:1673–82.
- [29] Du D, Darkwa J, Kokogiannakis G. Thermal management systems for photovoltaics (PV) installations: a critical review. *Sol Energy* 2013;97:238–54.
- [30] Micheli L, Sarmah N, Luo XC, Reddy KS, Mallick TK. Opportunities and challenges in micro- and nano-technologies for concentrating photovoltaic cooling: a review. *Renew Sustain Energy Rev* 2013;20:595–610.
- [31] Manual F. *Manual and user guide of Fluent Software*. Fluent Inc.; 2005.
- [32] Zhang QC, Simko TM, Deer CJ, Collins RE, Turner GM, Brunotte M, et al. The measurement and calculation of radiative heat transfer between uncoated and doped tin oxide coated glass surfaces. *Int J Heat Mass Transf* 1997;40:61–71.
- [33] Modest MF. *Radiative heat transfer*. Academic Press; 2013.
- [34] Sellami N, Meng XL, Xia XL, Knox AR, Mallick TK. Optical and heat transfer performance of a novel nonimaging concentrator. In: *Conference: CPV-11, France*; 2015.